Supporting Information

Wittemyer *et al.* 10.1073/pnas.0801744105

SI Text

Methods. We denote the time series of step length for individual i during time t-1 to t as $y_{i,t}$. The autocorrelation function of each $y_{i,\cdot}$ revealed clear cycling in the data, with peaks occurring at lags separated by more than 6 h, depending on the individual i. We estimated missing values using expected values from a Kalman smoother with a first-order autoregressive AR state-space model assuming mean zero Gaussian process noise, as well as mean zero Gaussian observation error (1). This smoothing imposed no artificial seasonal (in the parlance of time domain methods) cyclical structure to the data.

Spectral analysis is an effective tool for detecting frequencies υ driving periodic fluctuations in data time series, where the spectral density is defined as the Fourier transform of a time series autocovariance function (1). We obtained estimates of spectrums using smoothed periodograms using a modified Daniell smoother with adjacent three points, and a cosine bell-tapered $y_{i,\cdot}$, standard approaches to accommodate the inherent discreteness and finiteness of data when estimating spectral density functions (1). All analyses were done with R 2.6.1 software (2). To facilitate visual comparison with theoretical spectral densities of white and red noise, we normalized by the sample variance σ_i^2 for each $y_{i,\cdot}$. Under this normalization, the theoretical power spectrum is given by $1/(1 + \varphi^2 - 2\varphi\cos(\upsilon))$ for red noise and the constant 1 for white noise where φ is the lag-1 autocorrelation coefficient estimated separately from each data time series (1).

Periodograms assume stationarity in the data, giving time-averaged estimates of the frequency-dependent variance components, thereby precluding the identification of localized changes in the dominant frequencies in the periodograms, given their presence. Wavelet analysis has emerged as a useful tool for detecting temporal localization of frequencies explaining variation in stochastic time series data (3, 4). Using this technique with software in Maruan and Kurths (5), we computed the L^2-normalized continuous wavelet transforms of the $y_{i,\cdot}$,

$$W[b, a] = \sum_{k=1}^{T} \frac{1}{\sqrt{a}} \psi^*\left(\frac{k-b}{a}\right) y_{i,k}$$

for the analyzing (mother) wavelet, using the Morlet wavelet $\psi(t) = \pi^{1/4}\, e^{-i\omega_0 t} e^{-(t^2/2)}$, to obtain an estimate (called the scalogram) of the wavelet periodogram from the squared modulus values $W[b, a]^2$ without smoothing in either the time or scale directions. We chose $\omega_0 = 2\pi$ to preserve an inverse relationship between the scale of the analyzing wavelet and frequency, $a = 1/\upsilon$ (5). As suggested by Torrence and Compo (4), we chose scales δ_j, $j = 0, \ldots, J$, by setting the minimum scale $a_0 = 6$ h at twice the sampling interval, $\delta_j = 1/24$ and $J = 120$, giving a maximum scale of 64 days. This is the natural choice for the range of scales with the minimum being twice the sampling interval, and the maximum imposed by overall sample size. We bootstrapped 1000 replicate scalograms from the null AR(1) model to obtain 0.95 quantile values for significance testing when determining local patches of modulus values in the time frequency domain that were different from red noise (4, 5)—that is, had more complex autocorrelation structure than red noise. As described next, we used these significant patches in two ways to measure the emergence of complex autocorrelative structure in movement. Finally, assuming an identical stochastic process driving the movement time-series realizations for three categories of social ranking, the scalograms were averaged across individuals of the same social rank category to estimate the social group wavelet spectrum shown in Fig. 1.

To quantify a relative amount of autocorrelation structure at each time step not attributed to the null model of red noise, we used a Plancherel formula for wavelets. This formula for wavelets relates the total time-series variance σ_i^2 to the modulus values of the wavelet transform by $\langle W,W\rangle_H = TC_\psi\sigma_i^2$ (6), where

$$\langle u, v\rangle_{\mathrm{H}} := \int\int_{\mathbf{R}\times\mathbf{R}^*} u(a, b)v(a, b)\, \frac{da\,db}{|a|^2}$$

and C_ψ is a wavelet-specific constant. Thus, for each time step, we obtained the proportion of variance explained by scales inside significant patches

$$\sigma^2_{i,\mathrm{sig}}(b) = \int_{\mathbf{R}^*} \delta(a)\frac{|W[b, a]|^2}{a}\, da \Big/ \int_{\mathbf{R}^*} \frac{|W[b, a]|^2}{a}\, da,$$

where $\delta(a)$ is a Dirac measure taking on the value of 1 when a is inside a significant patch and 0 elsewhere. Averaging the $\sigma^2_{i,\mathrm{sig}}$ in blocks of time offers a relative measure of the degree of complex autocorrelation in movement across that block of time.

Simulation Study. To facilitate biological interpretation of the types of spectral results and time distributions of step lengths, we conducted a movement simulation study based on a stochastic partial differential equation model (7) from which to apply the statistical methods described herein. Following the notation in Brillinger *et al.* (7), we simulated positions $\mathbf{r}(t)$ in the x-y plane of an animal at time t given by using the stochastic differential equation $\mathbf{r}(t) = \mathbf{r}(0) + \int_0^t \mu(\mathbf{r}(s),s)\mathrm{d}s + \int_0^t \sigma(\mathbf{r}(s),s)d\mathbf{B}(s)$, where μ is the drift, σ is the dispersion, and $\mathbf{B}$ is a Wiener process. We simulated 100 paths $\mathbf{r}(t)$ for two different daily activity scenarios that elicit similar diurnal frequency signatures, characterized in Fourier and wavelet analyses results, to those found from movements of the studied elephants. For simulations, we considered t from 0 to 32 days, with $\mathbf{r}(t)$ incremented in 30 s steps and recorded at hourly intervals for the first 30 days. To simulate a simple rest-active daily activity behavior, we fit normal distributions to the logarithmic transformed velocity time series of M31 during the wet season for values below and above the 3/24 quantile (chosen from visual inspection of the data to roughly reflect an expected amount of resting time for these elephants). Values for the pairs $(\mu(\mathbf{r}(s), s), \sigma(\mathbf{r}(s), s))$ during resting and active activities were estimated at (2.67, 0.90) and (6.12, 0.95), respectively (turning angle is not considered, so the values are the same for the x and y dimensions). Each hour of each simulation day a random time value uniformly distributed on [0.5 h, 1.5 h] was selected. For the first three random times (with expected duration of 3 h), the simulation used the estimated rest parameters (2.67, 0.90), and the subsequent 21 random times (with expected durations of 21 h), the simulation used the estimated active parameters (6.12, 0.95). The results of this study are summarized in supporting information (SI) Fig. S2. To simulate the twice-a-day rest-active daily activity behavior, we used the M31 velocity time series during the dry season to obtain estimates of three behaviors: rest, low activity, and high activity. Parameters for these three behaviors were obtained by fitting a log-normal distribution to the dry season velocity time series of M31 for values below the 3/24 quantile, between the 3/24 and 5/6

quantiles, and above the 5/6 quantile, yielding parameter values of (2.47, 0.87), (5.52, 0.80), and (7.32, 0.35), for rest, low activity, and high activity, respectively. As before, each hour of each simulation day a random time value uniformly distributed on [0.5 h, 1.5 h] was chosen. The daily behavioral sequence with expected time duration was set at rest for 3 h, low activity for 4 h, high activity for 3 h, rest for 2 h, low activity for 3 h, high activity for 4 h, and low activity for 5 h. The results of this study are summarized in Fig. S3. A more complete evaluation of the Fourier and wavelet analyses for detecting behavioral constancy, cycling, randomness, change under differing biological scenarios (e.g., crepuscular activity or more complicated sequences of movement activity), and amounts of stochasticity, in both the distribution of duration of each movement activity and sampling interval, remain a subject of current research (8).

Additional Data Analyses. For each individual we obtained their smoothed periodograms (Fig. S1) and scalograms (Fig. S3), the latter of which was used for the subsequent analyses to evaluate hypotheses H1–H3 described in the main text. For individuals M54, M5, R28, R22, and M31, data at a 1 h sampling interval was available and we present their smoothed periodograms (Fig. S2) and scalograms (Fig. S4) for comparative purposes.

1. Shumway RH, Stoffer DS (2000) *Time Series Analysis and Its Applications* (Springer, Harrisonburg, VA), pp 213–333.
2. R Development Core Team (2007) *R: A Language and Environment for Statistical Computing* (R Foundation for Statistical Computing, Vienna).
3. Maraun D, Kurths J, Holschneider M (2007) Nonstationary Gaussian processes in wavelet domain: Synthesis, estimation, and significance testing. *Phys Rev E Stat Nonlin Soft Matter Phys*, 10.1103/PhysRevE.75.016707.
4. Torrence C, Compo GP (1998) A practical guide to wavelet analysis. *Bull Am Meteorol Soc* 79:61–78.
5. Maraun D, Kurths J (2004) Cross wavelet analysis: Significance testing and pitfalls. *Nonlin Proc Geophys* 11:505–514.
6. Blatter C (1998) *Wavelets: A Primer* (A K Peters, Natick, MA), pp 69–73.
7. Brillinger DR, Preisler HK, Ager AA, Kie JG (2004) An exploratory data analysis (EDA) of the paths of moving animals. *J Stat Plan Inference* 122:43–63.
8. Polansky L, Wittemyer G, Cross P, Tambling C, Getz WM. Characterizing animal movement and behavior using frequency and time-frequency domain time series methods. *Ecology*, in press.

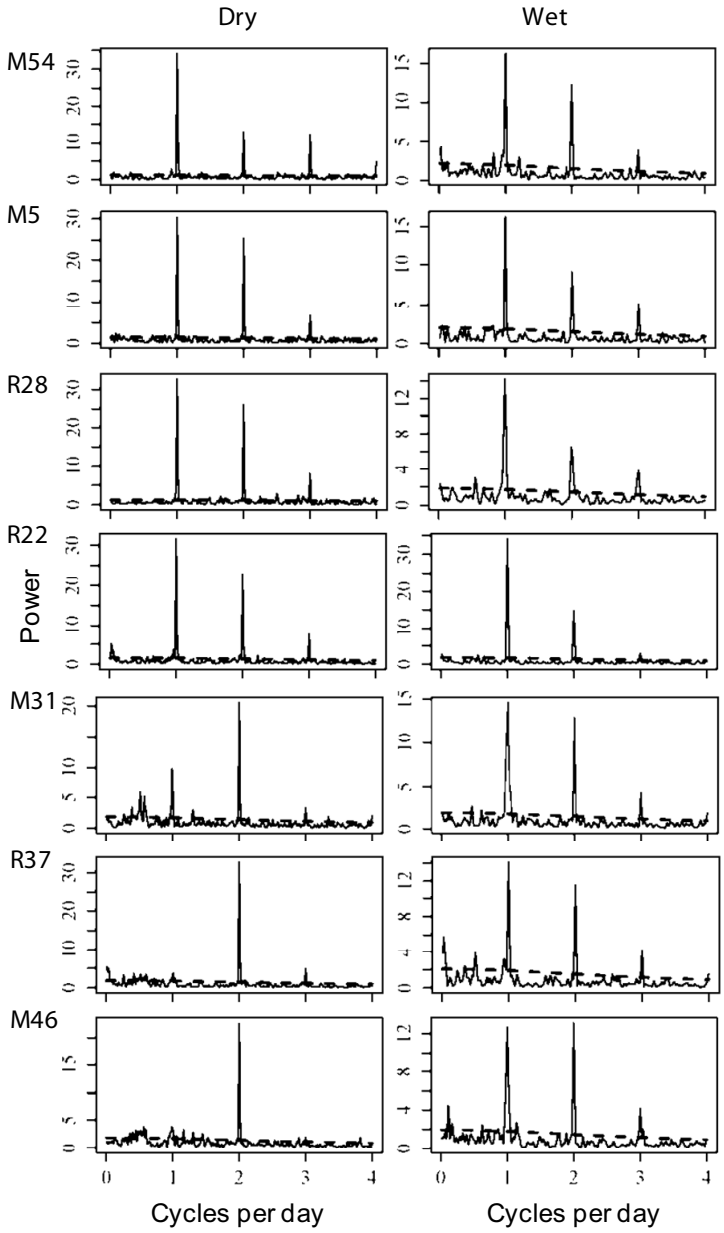

Fig. S1. Individual movement periodograms normalized so that white noise has a constant spectral density at 1 for individuals sampled every 3 h. Clear peaks in the periodograms above the theoretical red-noise spectral densities (dashed lines at the foot of the peaks) suggest relatively elaborate movement autocorrelation (these peaks remained significant as compared with Bonferroni corrected 95% confidence envelopes around the periodograms). Periodograms paired by individual show dominant cycles during the dry season (*Left*) and wet season (*Right*). Socially dominant individuals (M54, M5, R28) show little seasonal change in frequencies accounting for movement variation. In contrast, most lower-ranked individuals (M31, M46, R37) show clear seasonal differences in the dominant periodogram frequencies. The emergence of a similar spectral signature as the dominants during the wet season possibly relates to impacts of changes in resource abundance.

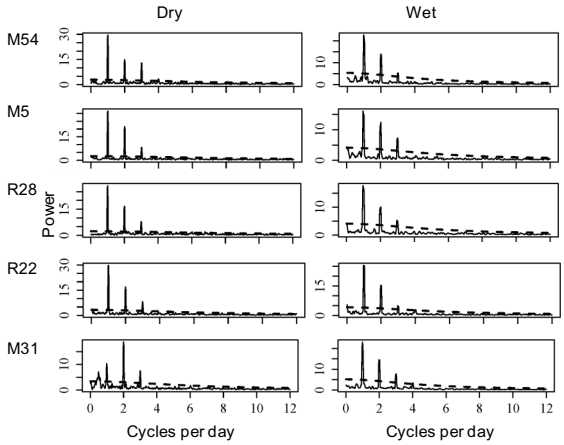

Fig. S2. Individual movement periodograms normalized so that white noise has a constant spectral density at 1 for the subset of five individuals whose location was sampled hourly, illustrating periodogram structure here is similar to that from the coarser sampling interval (Fig. S1). The dashed line shows the theoretical red-noise power spectrum.

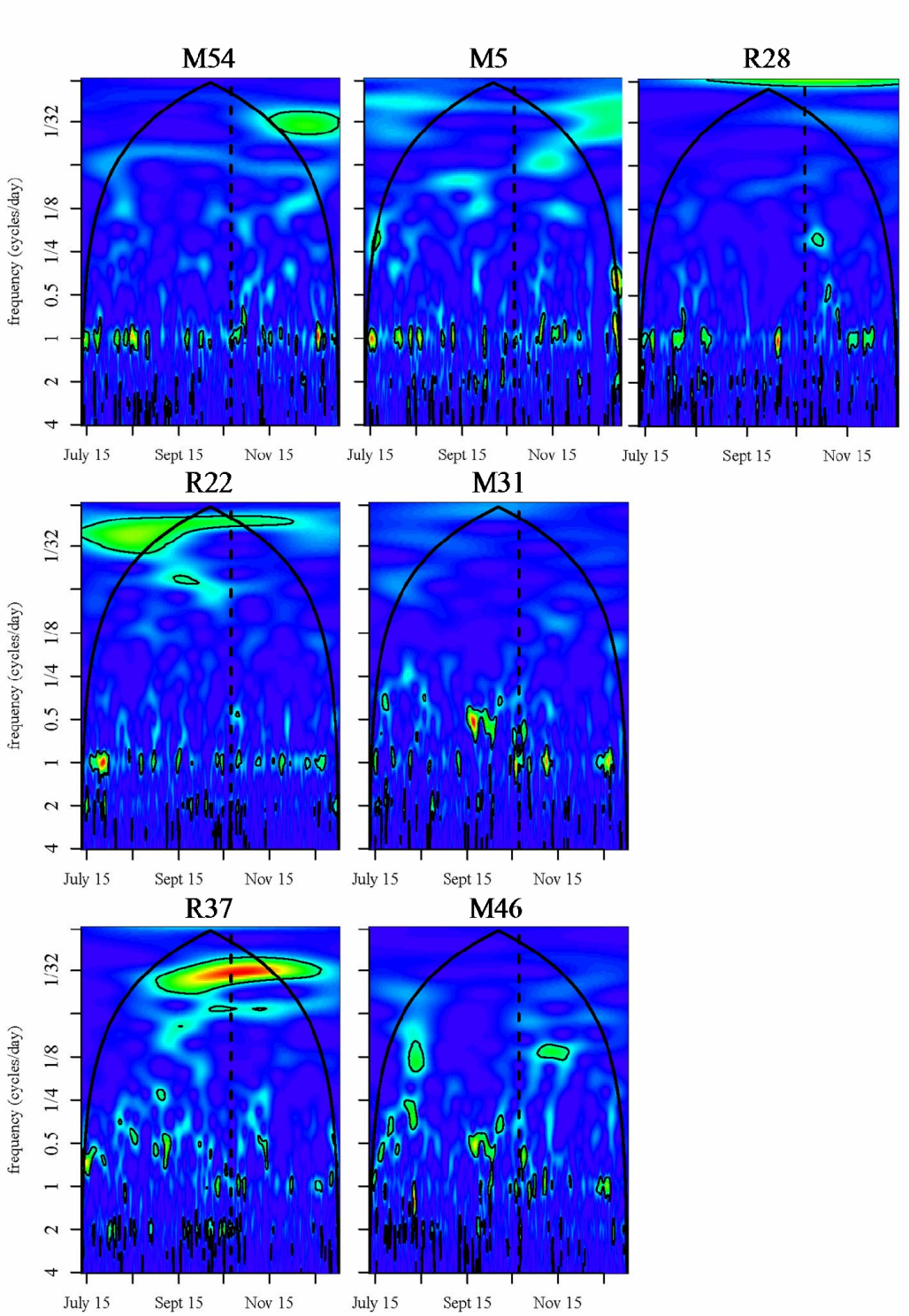

Fig. S3. Wavelet scalograms of natural logarithmic transformed net displacement time series of the seven individual elephants with locations sampled every 3 h. Larger squared modulus values correspond to warmer colors (values of 1 are given a red color) and smaller values corresponding to cooler colors (values of 0 are purple). The thick solid line denotes the cone of influence outside of which modulus values are affected by zero padding and should not be considered; the thick the vertical dashed line gives the approximate date of transition from the dry to wet season. The thin lines enclose regions of modulus values greater than or equal to the 0.95 sample quantile of 1000 bootstrapped scalograms of a red-noise null model fit to the data and are used to define the temporal regions of significant cycling referred to in the text. The first three scalograms are for the movements of dominants, the second two midranking, and the bottom two are for the lowest-ranking elephants.

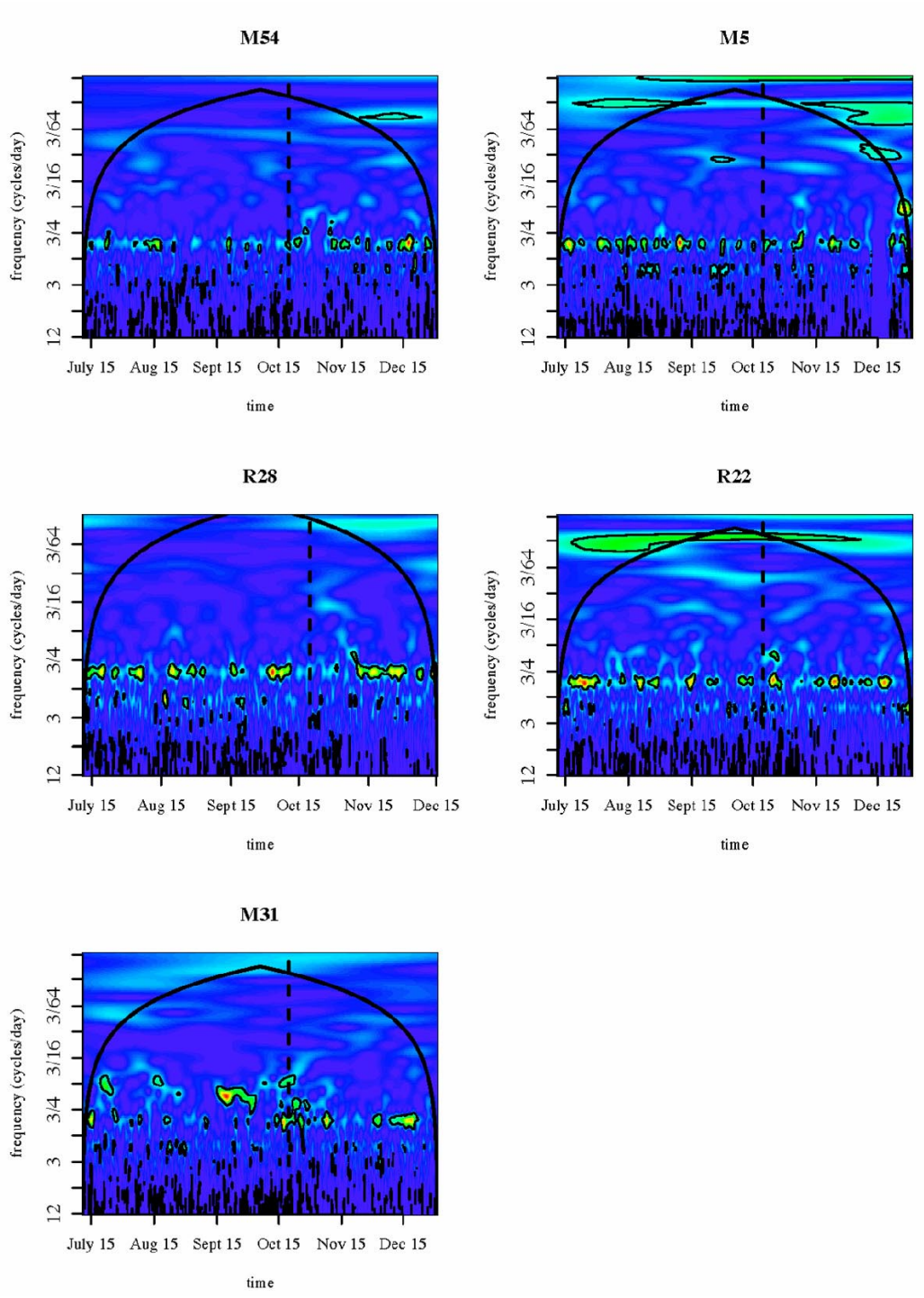

Fig. S4. Wavelet scalograms of natural logarithmic transformed net displacement time series for five individual elephants that had their locations sampled every hour, illustrating that the coarser sampling interval used in the main analysis for these five individuals does not change the findings about how the distribution of modulus power is distributed over frequencies or time (Fig. S3). Larger squared modulus values correspond to warmer colors (values of 1 are given a red color) and smaller values corresponding to cooler colors (values of 0 are purple). The thick solid line denotes the cone of influence outside of which modulus values are affected by zero padding and should not be considered; the thick vertical dashed line gives the approximate date of transition from the dry to wet season. The thin lines enclose regions of modulus values greater than or equal to the 0.95 sample quantile of 1000 bootstrapped scalograms of a red-noise null model fit to the data and are used to define the temporal regions of significant cycling referred to in the text.

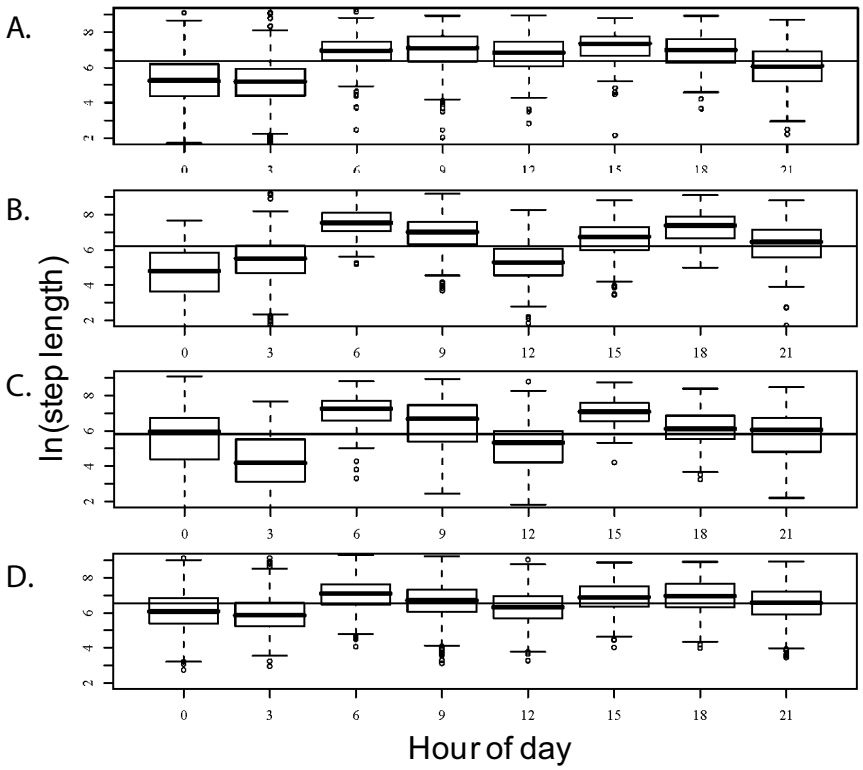

Fig. S5. Box plots of the distribution of log step lengths (meters) by hour of day drawn from time steps with significant wavelet modulus value at a particular frequency (*a*–*c*) or no significant frequency at all (*d*). Combined data from the seven elephants show that the differences in (*A*) one-, (*B*) two-, and (*C*) three-a-day cycles are driven by the timing of periods of rest and movement across a day. (*A*) Extended periods of low to no displacement (relating to sleeping cycles) occurring in the early morning, followed by moderate movements across the remaining diurnal period characterize one-a-day cycles of movement. (*B*) Two-a-day cycling is characterized by two periods of rest, the first approximately the same time as that in one-a-day cycles with the second occurring midday coinciding with the hottest time of the day. (*C*) Three-a-day cycles appear to be a modified version of (*b*) with different periodicity from the distributions associated with the previous frequencies. (*D*) Stepwise displacements during periods without cycling show attenuated periodicity not registered as significant in the analysis. Comparison of distributions from the same elephant shows the same, but stronger, differentiation.

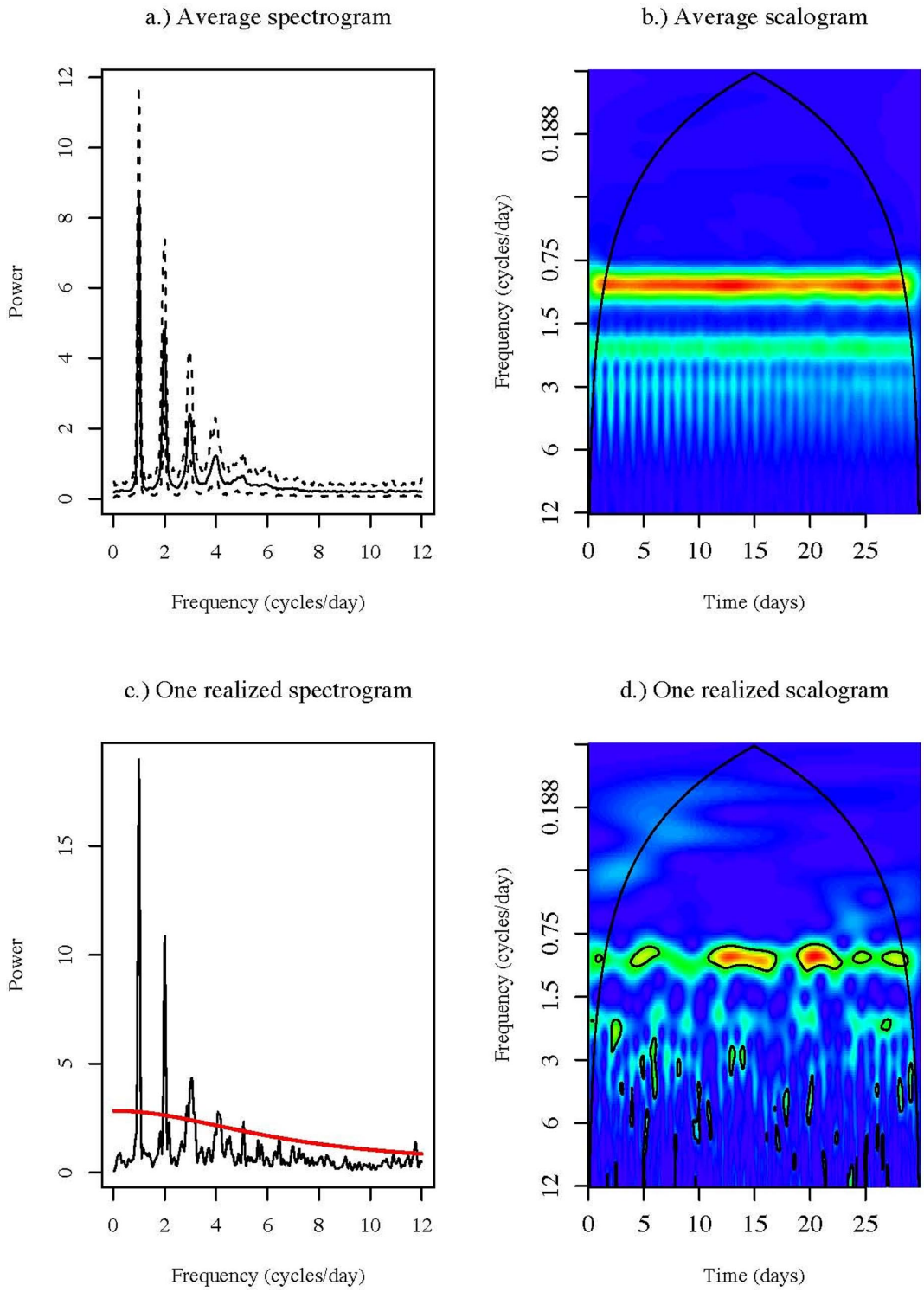

Fig. S6. Periodogram and scalogram structure for once-a-day rest diurnal activity from simulated data created using a simple two-mode model of rest and movement similar to the movement pattern shown in Fig. S5*A*. (*A*) Black solid line shows the average normalized periodogram with tapered data and smoothed using a modified Daniell smoother over the previous and subsequent three data points; lower and upper dashed lines give the 0.05 and 0.95 sample quantiles, respectively, of the power at each frequency. The theoretical white-noise spectrum is at 1 for all frequencies. (*B*) Normalized average scalogram of squared modulus values shown in color with 0 corresponding to purple and 1 corresponding to red, with the cone of influence (see text and ref. 4) given by the black line. (*C*) Smoothed periodogram for one realization of a movement path (black line) with the theoretical red-noise spectrum shown by the red line and the theoretical white noise taking values of 1 for all frequencies. (*D*) Using the same realized path $r(t)$ analyzed in (*C*), normalized squared modulus values for specific time-frequency values are shown in color, with 0 corresponding to purple and 1 corresponding to red. Thick solid line gives the cone of influence; thin solid lines contain regions of significant squared modulus values different from red noise (5).

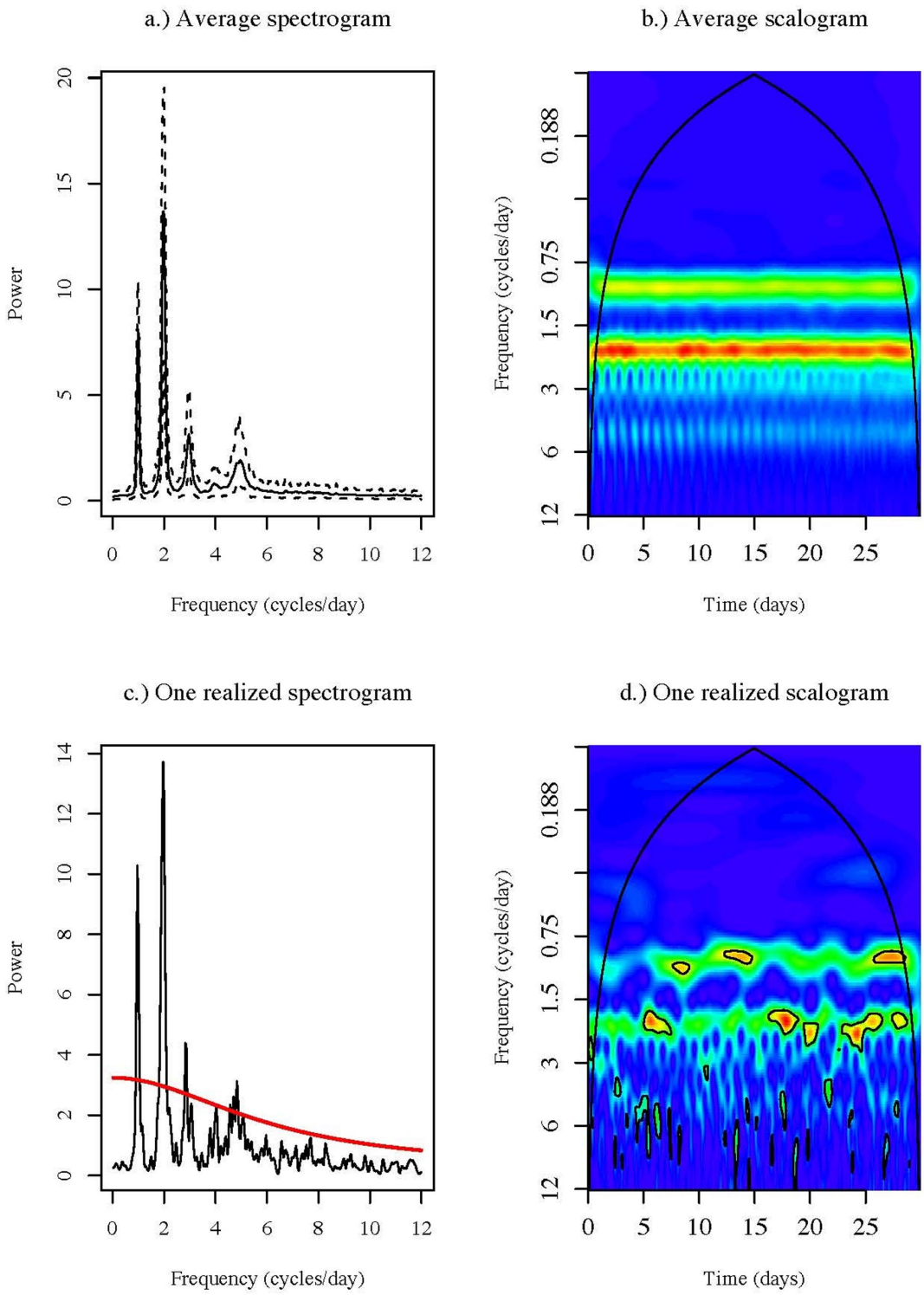

Fig. S7. Periodogram and scalogram structure for twice-daily rest diurnal activity from simulated data created using a simple two-mode model of rest and movement similar to the movement pattern shown in Fig. S5*B*. (*A*) Black solid line shows the average normalized periodogram with tapered data and smoothed using a modified Daniell smoother over the previous and subsequent three data points; lower and upper dashed lines give the 0.05 and 0.95 sample quantiles, respectively, of the power at each frequency. The theoretical white noise spectrum is at 1 for all frequencies. (*B*) Normalized average scalogram of squared modulus values shown in color with 0 corresponding to purple and 1 corresponding to red, with the cone of influence (see text and ref. 4) given by the black line. (*C*) Smoothed periodogram for one realization of a movement path r(*t*) (black line) with the theoretical red-noise spectrum shown by the red line and the theoretical white noise taking values of 1 for all frequencies. (*D*) Using the same realized path **r**(*t*) analyzed in panel (*C*), normalized squared modulus values for specific time-frequency values are shown in color with 0 corresponding to purple and 1 corresponding to red. Thick solid line gives the cone of influence; thin solid lines contain regions of significant squared modulus values different from red noise (5).

Table S1. Proportion of variation in movement data explained by autocorrelation calculated for blocks of time coinciding with NDVI sampling intervals

Date	M54	M5	R28	R22	M31	M46	R37	Avg
11 July 2001	0.42	0.41	0.41	0.35	0.28	0.24	0.35	0.35
21 July 2001	0.22	0.03	0.20	0.53	0.25	0.26	0.24	0.25
1 August 2001	0.34	0.37	0.45	0.08	0.29	0.41	0.29	0.32
11 August 2001	0.46	0.35	0.47	0.18	0.15	0.29	0.17	0.30
21 August 2001	0.30	0.23	0.23	0.15	0.27	0.20	0.22	0.23
1 September 2001	0.23	0.31	0.11	0.10	0.14	0.27	0.23	0.20
11 September 2001	0.20	0.16	0.15	0.25	0.40	0.35	0.20	0.24
21 September 2001	0.29	0.30	0.25	0.20	0.39	0.43	0.24	0.30
1 October 2001	0.04	0.13	0.43	0.25	0.26	0.20	0.38	0.24
11 October 2001	0.07	0.26	0.16	0.31	0.36	0.19	0.46	0.26
21 October 2001	0.23	0.08	0.29	0.21	0.25	0.29	0.27	0.23
1 November 2001	0.17	0.19	0.20	0.07	0.29	0.17	0.08	0.17
11 November 2001	0.11	0.18	0.25	0.11	0.10	0.18	0.16	0.16
21 November 2001	0.11	0.21	0.34	0.15	0.09	0.05	0.13	0.15
1 December 2001	0.19	0.23	0.10	0.06	0.06	0.03	0.03	0.10
11 December 2001	0.27	0.04	0.21	0.20	0.47	0.31	0.17	0.24
21 December 2001	0.14	0.51	NA	0.23	0.14	0.16	0.22	0.23

Data were averaged across all individuals, offering a metric of when autocorrelation in movements of the population was comparatively strong or weak.

Table S2. Proportion of time (in percentages) that individuals produced autocorrelated movements significantly larger than expected compared with best-fitting red noise at the indicated frequencies (≤1 and >1 cycles per day) and seasons, within and outside the park

		Dry season				Wet season			
		≤1 cycle/day		>1 cycle/day		≤1 cycle/day		>1 cycle/day	
Rank	ID	In	Out	In	Out	In	Out	In	Out
High	M54*	64	NA	0	NA	40	39	0	0
High	M5	48	53	0	0	35	61	0	0
High	R28*	55	NA	0	NA	52	25	0	0
Mid	R22	61	36	0	0	74	81	0	0
Mid	M31	48	31	0	30	18	64	0	0
Low	R37	79	29	2	14	73	28	0	9
Low	M46	36	32	16	28	21	62	31	32

*These elephants spent less than 1% of their time outside protected areas during the dry season.

Table S3. Proportion of days that elephants visited permanent water sources

ID	Dry, %	Wet, %
M54	90	56
M5	97	84
R28	95	72
R22	90	66
M31	72	48
R37	83	34
M46	78	42

Note that percentages are significantly greater during the dry than the wet season.

Table S4. Proportion of time (across all frequencies) in which movement autocorrelation was significantly different from red noise

Rank	ID	Proportion of time in cyclic movements (%)
High	M54	55
High	M5	49
High	R28	52
Mid	R22	66
Mid	M31	51
Low	R37	47
Low	M46	53

An AR(1) model was calculated from wavelet results, showing similar proportions of the elephants' movements were autocorrelated regardless of social status.